

# Reflectors Tune Near-Field Thermal Transport

Yun-Chao Hao,<sup>1,2</sup> Matthias Krüger,<sup>3,\*</sup> Mauro Antezza,<sup>4,5</sup>  
Cheng-Long Zhou,<sup>1,2</sup> Hong-Liang Yi,<sup>1,2</sup> and Yong Zhang<sup>1,2,†</sup>

<sup>1</sup>*School of Energy Science and Engineering, Harbin Institute of Technology, Harbin 150001, China*

<sup>2</sup>*Key Laboratory of Aerospace Thermophysics, Ministry of Industry and Information Technology, Harbin 150001, China*

<sup>3</sup>*Institute for Theoretical Physics, University of Göttingen, 37077 Göttingen, Germany*

<sup>4</sup>*Laboratoire Charles Coulomb(L2C), UMR 5221 CNRS-Université Montpellier, F-34095 Montpellier, France*

<sup>5</sup>*Institut Universitaire de France, 1 rue Descartes, F-75231 Paris Cedex 05, France*

(Dated: September 20, 2024)

We explore near-field thermal radiation transport in nanoparticles embedded within a multilayer slab structure, focusing on dynamic modulation of heat flux via cavity interactions. Our findings reveal that by tuning the distance between reflectors and nanoparticles, thermal transport can be significantly suppressed or enhanced, driven by selective excitation of surface modes within the cavity. By precisely adjusting inter-slab gaps, we achieve multi-order control over thermal flux while maintaining stability across a broad range of configurations. Notably, internal slab arrangement plays a pivotal role, with compact designs yielding the most pronounced effects. This work unveils a novel mechanism for manipulating near-field heat transfer, with exciting potential for nanoscale thermal management and thermal sensing technologies.

Advancements in nanotechnology and near-field radiative heat transfer (NFRHT) have made high-sensitivity mK-level temperature detection essential for microelectromechanical systems [1–4], including slab structures [5–9] and spherical structures [10–13]. As efficient thermal feedback platform [14–17], nanoparticles exhibit local thermal enhancements in multi-particle arrangements [18–21], suggesting their suitability for near-field thermal information relay, bolstered by levitated nanoparticles [22]. However, NFRHT efficiency in particle structures is dampened by the distance-proportional law  $d^{-6}$  [23] (where  $d$  represents the separation distance), and in slab structures by  $d^{-2}$  [24], indicating challenges in long-range thermal transport. Introducing slabs between particles can provide additional thermal exchange channels [25–27], akin to the enhancement effects seen in multi-layer slab structures [28–31], potentially supported by the  $d^{-3}$  law that particle and slab structures follow as a function of distance  $d$  [32]. Incorporating intermediate slabs significantly boosts radiative heat transfer efficiency in nanoparticle assemblies but offers limited tunability [25–27].

The study of electromagnetic wave interactions with matter in a cavity has greatly advanced fields like cavity quantum electrodynamics [33, 34] and cavity optomechanics [35, 36]. In the domain of NFRHT, substantial research has been devoted to controlling heat flux by adjusting the gap with the cavity acting as a thermal source [37–39]. However, the use of cavity modes as a mechanism to modulate heat exchange of substances (typically nanoparticles) within the cavity has not yet been studied. Here, we introduce reflective slabs *on the outside* of the nanoparticles to form a cavity structure, allowing us to control the radiative properties by tuning the cavity parameters [see Fig.1(a)]. A central slab of thickness  $\delta$ , termed ‘repeater’, is shown to greatly

enhance thermal flux when outer (semi-infinite) surfaces, termed ‘reflectors’, are at a large distance. Depending on distance, these reflectors select the dominant surface modes (SPhPs) [40, 41], thereby tuning the transfer between the nanoparticles. Particles and slabs are made of non-magnetic dielectric materials. This thus introduces a novel method of selecting modes and thereby tuning near-field transfer.

The spatial arrangement is shown in Fig.1(a) with the nanoparticles having distances  $l$  and  $d$  from the repeater and reflector, respectively. With the entire setup at temperature  $T$  and particle 1 warmed to  $T + \Delta T$  (where  $T \gg \Delta T$ ),  $\Delta T$  causes radiative energy exchange, where we here focus on transfer  $\Phi$  from particle 1 to particle 2, with  $\Delta T > 0$  [42, 43]. For particle radius  $R \ll \lambda_T$  (thermal wavelength  $\lambda_T = c\hbar/k_B T$ ) and  $R$  small compared to  $l$  and  $d$ , particles are approximated as dipoles [44]. Accordingly, the interparticle thermal conductance  $H = \partial\Phi/\partial T$  follows [18, 45, 46]

$$H = 64\pi^2 \int_0^\infty \frac{d\omega}{2\pi} \hbar \omega n' k_0^4 \text{Im}(\alpha_1) \text{Im}(\alpha_2) \text{Tr}(\mathbb{G}\mathbb{G}^\dagger), \quad (1)$$

where  $\omega$  and  $k_0 = \omega/c$  respectively represent the angular frequency and the free space wave number.  $n'$  is the derivative of the Bose-Einstein distribution  $n = [\exp(\hbar\omega/k_B T) - 1]^{-1}$  with respect to  $T$ .  $\alpha_i(\omega) = R_i^3[\varepsilon_i(\omega) - 1]/[\varepsilon_i(\omega) + 2]$  is the particles’ electrical polarizability with  $\varepsilon(\omega)$  the dielectric permittivity [47].

$\mathbb{G}$  refers to the dyadic Green’s function (DGF), which characterizes the electromagnetic interaction between two particles. In the Fourier-transformed two-dimensional wavevector space, due to the symmetry of the transverse structure, we obtain

$$\mathbb{G} = \int_0^\infty \frac{dk_\rho}{2\pi} k_\rho g, \quad (2)$$

where  $k_\rho$  is the transverse wave number, with the relationship  $k_z = \sqrt{k_0^2 - k_\rho^2}$  and  $g$  is given by

$$g = \frac{i}{4k_z k_0^2} \begin{pmatrix} k_z^2 \alpha + k_0^2 \beta & 0 & 0 \\ 0 & k_z^2 \alpha + k_0^2 \beta & 0 \\ 0 & 0 & 2k_\rho^2 \gamma \end{pmatrix}. \quad (3)$$

Here we introduced abbreviations

$$\begin{aligned} \alpha &= (A^{TM} - C^{TM})e^{ik_z l} + (D^{TM} - B^{TM})e^{-ik_z l} \\ \beta &= (A^{TE} + C^{TE})e^{ik_z l} + (D^{TE} + B^{TE})e^{-ik_z l}, \\ \gamma &= (A^{TM} + C^{TM})e^{ik_z l} + (D^{TM} + B^{TM})e^{-ik_z l} \end{aligned} \quad (4)$$

where coefficients  $A - D$  denote the field amplitudes constituting the Weyl components of DGF. The superscripts TM and TE denote the polarization (see supplementary materials [48] for details).

To simplify the analysis, we fix  $T = 300$  K,  $l = 100$  nm,  $\delta = 3 \mu\text{m}$ , and  $R_1 = R_2 = 5$  nm, and vary the distance  $d$ . The impact of  $\delta$  is discussed in the supplementary materials [48]. The material properties of the particles and slabs are chosen carefully: The resonance frequency for surface localized modes of the particle are determined by the polarizability condition  $\varepsilon(\omega_{np}) + 2 = 0$ . The chosen isotropic SiC particles [49] show that  $\omega_{np}$  is  $1.756 \times 10^{14}$  rad s $^{-1}$ . For the slabs, the SPhPs resonance, defined by  $\varepsilon(\omega_{sp}) + 1 = 0$  [50], yields  $\omega_{sp} = 1.787 \times 10^{14}$  rad s $^{-1}$  for SiC, which does not perfectly match with  $\omega_{np}$ ; surface mode coupling between particles and slabs of identical material invariably leads to monochromaticity loss [51, 52]. To address this, we exploit the Mie resonance effect [53, 54] to select slab materials with  $\omega_{sp}$  closely matching that of SiC particles, i.e.,  $\omega_{sp} \simeq \omega_{np}$  (for details see the supplementary materials [48]). Adjustments to  $\omega_{sp}$ , to finely tune resonance without altering peak values, are explored through isotope effects [55, 56], photonic crystal structures [26, 27], among other strategies [29].

The modification of an emitter's electromagnetic environment can enhance or suppress its interaction with light, a phenomenon known as the Purcell effect. By engineering the electromagnetic environment (e.g., through cavity design), one can control the coupling strength. We here study the influence of reflectors along the  $z$ -axis, with Fig. 1(b) showing thermal transport as a function of distance  $d$ . To understand the influence of the interior slab, we consider a reflectors-only configuration (model I) and contrast it with the setup depicted in Fig. 1(a) (model II). In model I, when the reflectors are distant from the particles ( $d = 10 \mu\text{m}$ ), evanescent modes become ineffective when crossing the vacuum, causing  $H$  to approach  $H_0$ , the value found for two nanoparticles in empty space. The oscillations observed are due to the mutual reflection of propagating photons between slabs. As the reflectors approach the particles, i.e., with decreasing  $d$ ,  $H$  strongly increases, by two

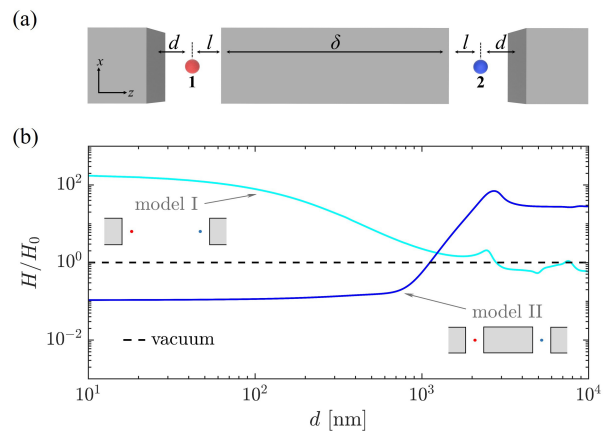


FIG. 1. (a) Diagram illustrating near-field thermal transport between particles 1 and 2, mediated by slabs. The 'repeater' is the intermediate slab with thickness  $\delta$ , and the 'reflectors' are the adjacent semi-infinite slabs, with their distances from the particles labeled  $l$  and  $d$ , respectively. (b) Compares the thermal conductance  $H$  of different systems, normalized to vacuum conductance  $H_0$ , as functions of the distance  $d$  between the reflectors and particles. Models I (only reflectors) and II (repeater and reflectors) are shown.

orders of magnitude. We attribute this enhancement to surface modes (SPhPs), highlighting the reflectors' role in boosting particle thermal transport, consistent with related research findings [57–59]. In model II, with the reflectors distant from the particles, photon-induced oscillations are minimal relative to the enhancement from the repeater's surface modes, making the curve essentially independent of  $d$ . This effectively equates to having only the repeater involved in heat exchange, with its enhancement effect aligning with related research findings [25–27]. Interestingly, moving the reflectors closer reduces  $H$  by three orders of magnitude, even below  $H_0$ , which suggests potential thermal flow suppression in compact configurations and challenges conventional understanding [60, 61]. This configuration-selective thermal channeling suggests that near-field thermal management devices, like thermal switches, can robustly control thermal flux through cavity gap adjustments, without moving the heat source. Notably, within the approximate ranges of  $d \lesssim l$  or  $d \gtrsim \delta$ , each configuration exhibits thermal flux nearly independent of  $d$ , akin to radiative heat transfer saturation under multi-body effects [62]. This implies that controlling thermal flux between particles by altering cavity gaps is largely robust.

Coupling strength shifts between particle and slab structure during thermal exchange depend on cavity mode and particle resonance frequency matching. The behavior of  $H$  with respect to  $d$  as shown in Fig. 1(b) is elucidated by examining the dispersion in momentum space. We therefore consider  $h(\omega, k_\rho)$  to characterize the distribution of  $H$  in momentum space and frequency

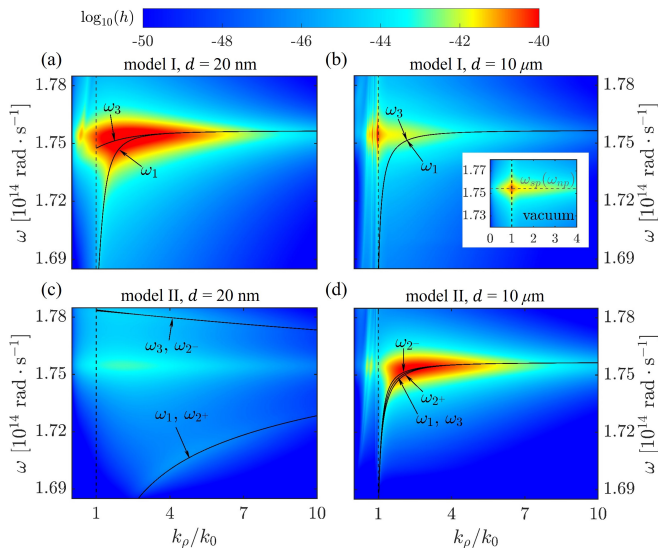


FIG. 2.  $h$  maps for models I and II at different  $d$ . Solid lines indicate system's cooperative surface modes dispersion curves; dotted lines separate free-space propagating ( $k_\rho < k_0$ ) and evanescent ( $k_\rho > k_0$ ) modes. Inset illustrates  $h$  map in vacuum.

domain, given by

$$h = 64\pi^2 \hbar \omega n' k_0^4 \text{Im}(\alpha_1) \text{Im}(\alpha_2) k_\rho \text{Tr}(Gg^\dagger + gG^\dagger) \quad (5)$$

with  $H = \int_0^\infty \frac{d\omega}{2\pi} \int_0^\infty \frac{dk_\rho}{2\pi} h(\omega, k_\rho)$  and

$$G = \int_0^{k_\rho} \frac{dk_\rho}{2\pi} k_\rho g. \quad (6)$$

Fig. 2(a) and (b) illustrate  $h$  as function of  $\omega$  and  $k_\rho$  for model I at  $d = 20$  nm and  $10 \mu\text{m}$ , respectively. Due to the overwhelming thermal flux provided around the above mentioned resonance frequencies [63], we focus on the range of frequencies around them. In this region, SPhPs are excited solely by TM polarized waves [64],  $\beta \simeq 0$  in Eq. (3), and we consider the dispersion curves in the evanescent mode region that are derived from the Fabry-Pérot-like denominator term

$$1 - R_+^{TM} R_-^{TM} e^{2ik_z(l+d)} = 0. \quad (7)$$

$R_+^{TM}$  and  $R_-^{TM}$  are the reflection coefficients at the interfaces of the repeater and reflectors within the vacuum gap surrounding the particles, respectively (see the supplementary materials for details [48]).

When the reflectors are close to the particles ( $d = 20$  nm), the optical distance between their interfaces approaches the inter-particle distance. The direct thermal emission and SPhPs received by particle 2 have comparable magnitudes. Under the coherent action of the reflectors' surface modes, the dispersion lines manifest as two symmetric and antisymmetric dispersion lines, denoted as  $\omega_1$  and  $\omega_3$ . These lines tend towards

degeneracy with increasing  $k_\rho$  and reducing penetration depth [43, 63]. By comparing with the  $h$  distribution in vacuum shown in the inset, Fig. 2(b), one can observe a distinct bright band near the dispersion curves, indicative of monochromatic enhancement at the  $\omega_{sp}$ . When the reflectors are distant from the particles ( $d = 10 \mu\text{m}$ ), the surface modes can no longer couple due to their inability to tunnel through the vacuum gap, resulting in  $\omega_1$  and  $\omega_3$  degenerating into the dispersion curve of a single interface. Here, the magnitude of SPhPs received by particle 2 is markedly less than direct thermal emissions from particle 1, with multiple bright bands formed by Fabry-Pérot-like standing waves emerging in the propagating mode region [64], correlating with fluctuations observed in Fig. 1(b).

Fig. 2(c) and (d) discuss model II under the same conditions, where the addition of a single-layer repeater introduces two new dispersion lines, denoted  $\omega_{2+}$  and  $\omega_{2-}$ . Close proximity between reflectors and particles extends symmetric and antisymmetric dispersion lines over a broader frequency due to surface modes coupling through the small vacuum gap, similar to Rabi splitting in quantum cavity [65, 66]. Moreover, due to the repeater's sufficient thickness,  $\omega_1$  and  $\omega_{2+}$ ,  $\omega_3$  and  $\omega_{2-}$  become degenerate. Behind this structural effect lies a wavenumber selective mechanism, monochromatic thermal emission from particle 1 spreads across the entire strong reflection band, while high- $k_\rho$  thermal channels close, hindering surface mode coupling within the repeater and suppressing monochromatic emission (for specific details, see the supplementary materials [48]).

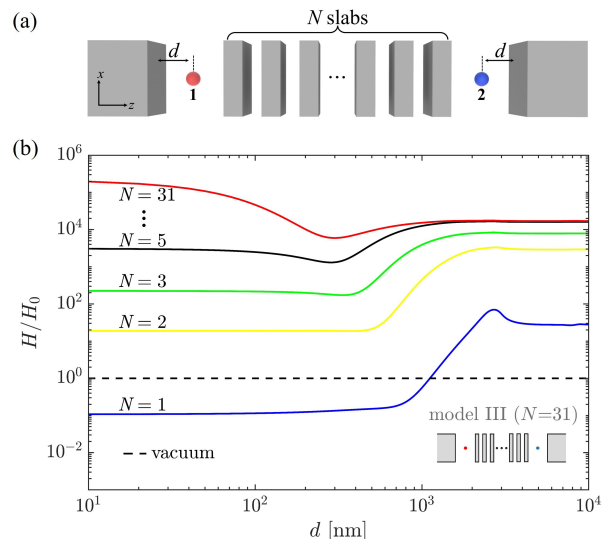


FIG. 3. System with a periodic multilayer repeater consisting of  $N$  slabs and  $N - 1$  vacuum layers, each with a thickness of  $\delta/(2N - 1)$ . (b) Shows how heat transfer coefficient  $H$  varies with distance  $d$  between the reflectors and particles across different  $N$  configurations.

This reveals the high tunability of thermal transport in model II and implies that adding more slabs does not inherently boost thermal radiation transport [67]. When the reflectors are distant, the coherent action within the vacuum gap vanishes, causing the surface mode dispersion lines  $\omega_1$  and  $\omega_3$  supported by the reflectors to degenerate back into a single interface dispersion, and  $\omega_{2+}$  and  $\omega_{2-}$  supported by the repeater to recouple into a single thin-film dispersion, showing thermal flux enhancement akin to that seen in Fig. 2(a).

Clearly, for a single-layer repeater, sufficient thickness ensures the distance of energy transmission but limits the tunneling of high- $k_\rho$  evanescent modes. Considering this, we explored a periodic multilayer repeater interspersed with vacuum layers [see Fig. 3(a)] to enhance surface electromagnetic mode utilization. This multilayer repeater, with slabs count  $N$  and total thickness  $\delta$ , essentially acts as a hyperbolic metamaterial (HMM), supporting coherent thermal transport of broad bandwidth hyperbolic modes over several magnitudes greater penetration depth than surface modes [68, 69]. Fig. 3(b) illustrates  $H$ 's dependence on  $d$  and  $N$ . Considering the impact on material properties, we limit  $N$  to a maximum of 31, designating the system as model III. When the reflectors are distant from the particles,  $H$  surpasses model II, benefiting from the multilayer's hyperbolic modes [26, 27]. As the reflectors approach the particles,  $H$  increases by an order of magnitude, underscoring reflectors' role in boosting thermal transfer. Increasing  $N$  effects a transition from the blue to the red line in Fig. 3(b), indicating that the configuration of the repeater alone can significantly increase thermal flow, and the joint action of the repeater and reflectors can

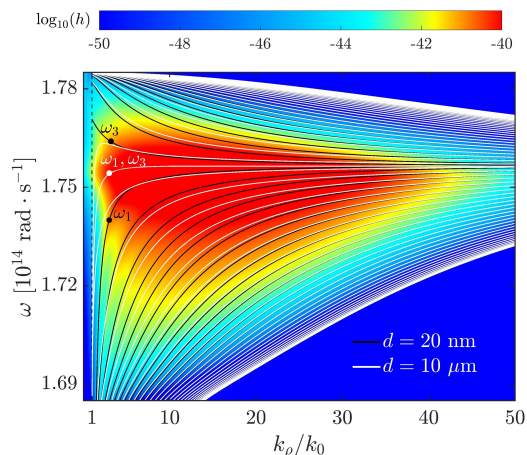


FIG. 4. The  $h$  map for model III at  $d = 20$  nm shows coupled surface wave dispersion lines. Black and white solid lines represent the cases for  $d = 20$  nm and  $d = 10 \mu\text{m}$ , respectively. Dispersion lines  $\omega_1$  and  $\omega_3$  are introduced by reflectors, with the remaining solid lines introduced by the multilayer repeater.

further extend the modulation range, even suppressing thermal flow. This demonstrates the system's capability to customize thermal flow based on the internal structure of the repeater and the position of the reflectors, enabling enhanced or suppressed thermal flow modulation in compact configurations without compromising system robustness. It opens promising pathways for thermal management and other fields.

Model III demonstrates enhanced thermal flow with closer reflectors compared to model II, as shown by the  $h$  distribution for model III at  $d = 20$  nm in Fig. 4, showing a significant improvement in penetration depth over models I and II. This enhancement stems from the coupling of short-range SPhPs at the HMM interface, facilitating high- $k_\rho$  thermal transport. Bragg scattering within the periodic photonic crystal alternately strengthens or weakens wave coherence, creating photonic band gaps. The  $2(N + 1)$  solid lines based on Eq. (7) represent the dispersion curves of cooperative surface modes, where  $\omega_1$  and  $\omega_3$  are the two dispersion lines introduced by the reflectors, and the remaining  $2N$  dispersion lines are introduced by the repeater. The black and white lines depict the cases for  $d = 20$  nm and  $d = 10 \mu\text{m}$ , respectively. It is evident that the black lines are pushed to higher- $k_\rho$  regions due to the coupling of surface modes within the vacuum gap. Hence, as the reflectors approach the particles, the outward expansion of the dispersion lines supported by the multilayer repeater leads to monochromatic loss in thermal flux, which is compensated by the introduction of dispersion lines supported by the reflectors. This explains the fluctuating behaviour of the red curve in Fig. 3(b). Despite model III featuring multiple thermal exchange channels, each channel's thermal transfer probability is much smaller than model II's single channel (for specific details, see the supplementary materials [48]). The enhancement of thermal flux is fundamentally due to the increase in penetration depth.

In summary, we discover novel tunability of transfer through multilayer slab structures via controlling the dominant transverse wavevectors using outside reflector surfaces. We showed how this can be used to tailor transfer by matching or de-matching modes in various geometries, including single or multilayer configurations with robust properties. The mechanical motion of the cavity can be achieved using a nanoscale displacement platform or an optomechanical cavity [35], and even extended to develop nanoscale mechanical vibration sensing systems driven by thermal information. The impact of the single-side reflector's motion is detailed in the supplementary materials [48]. This has promising implications for micro/nanoscale thermal radiation [70, 71], levitation dynamics [72, 73], local responses in sub-micron gaps [74, 75], thermal relaxation in compact nanostructures [76, 77], and Casimir interactions between nanoparticles and slabs [78, 79], among others.

This work was supported by the National Natural Science Foundation of China (Grant No. 52076056, No. U22A20210). M.K. acknowledges the support from the Volkswagen Foundation through SPRUNG. M.A. acknowledges the grant “CAT”, No. A-HKUST604/20, from the ANR/RGC Joint Research Scheme sponsored by the French National Research Agency (ANR) and the Research Grants Council (RGC) of the Hong Kong Special Administrative Region.

---

\* [matthias.kruger@uni-goettingen.de](mailto:matthias.kruger@uni-goettingen.de)

† [yong.zhang@hit.edu.cn](mailto:yong.zhang@hit.edu.cn)

- [1] S. Lang, G. Sharma, S. Molesky, P. U. Kränzien, T. Jalas, Z. Jacob, A. Y. Petrov, and M. Eich, Dynamic measurement of near-field radiative heat transfer, *Sci. Rep.* 7 (2017).
- [2] X. Luo, H. Salihoglu, Z. Wang, Z. Li, H. Kim, X. Liu, J. Li, B. Yu, S. Du, and S. Shen, Observation of near-field thermal radiation between coplanar nanodevices with subwavelength dimensions, *Nano Lett.* 24 (2024).
- [3] S.-A. Biehs, R. Messina, P. S. Venkataram, A. B. Rodriguez, J. Cuevas, and P. Ben-Abdallah, Near-field radiative heat transfer in many-body systems, *Rev. Mod. Phys.* 93 (2021).
- [4] G. Bimonte, T. Emig, M. Kardar, and M. Krüger, Nonequilibrium fluctuational quantum electrodynamics: Heat radiation, heat transfer, and force, *Annu. Rev. Condens. Matter Phys.* 8, 119 (2017).
- [5] A. Fiorino, D. Thompson, L. Zhu, B. Song, P. Reddy, and E. Meyhofer, Giant enhancement in radiative heat transfer in sub-30 nm gaps of plane parallel surfaces, *Nano Lett.* 18, 3711 (2018).
- [6] A. Fiorino, D. Thompson, L. Zhu, R. Mittapally, S.-A. Biehs, O. Bezencenet, N. El-Bondry, S. Bansropun, P. Ben-Abdallah, E. Meyhofer, and P. Reddy, A thermal diode based on nanoscale thermal radiation, *ACS Nano* 12, 5774 (2018).
- [7] L. Rincón-García, D. Thompson, R. Mittapally, N. Agraït, E. Meyhofer, and P. Reddy, Enhancement and saturation of near-field radiative heat transfer in nanogaps between metallic surfaces, *Phys. Rev. Lett.* 129 (2022).
- [8] R. Mittapally, J. W. Lim, E. Meyhofer, P. Reddy, and B. Song, Quantifying the effect of nanofilms on near-field radiative heat transfer, *ACS Photonics* 10, 2474 (2023).
- [9] R. Mittapally, J.-H. Lim, L. Zhang, O. D. Miller, P. Reddy, and E. Meyhofer, Probing the limits to near-field heat transfer enhancements in phonon-polaritonic materials, *Nano Lett.* 23, 2187 (2023).
- [10] Y. Shen, Y. Luan, J.-H. Lim, R. Mittapally, A. Reihani, Z. Wang, Y. Tsurimaki, S. Fan, P. Reddy, and E. Meyhofer, Surface phonon polariton-mediated near-field radiative heat transfer at cryogenic temperatures, *Phys. Rev. Lett.* 131 (2023).
- [11] B. Song, Y. Ganjeh, S. Sadat, D. Thompson, A. Fiorino, V. Fernández-Hurtado, J. Feist, F. J. Garcia-Vidal, J. C. Cuevas, P. Reddy, and E. Meyhofer, Enhancement of near-field radiative heat transfer using polar dielectric thin films, *Nat. Nanotechnol.* 10, 253 (2015).
- [12] J. Shi, B. Liu, P. Li, L. Y. Ng, and S. Shen, Near-field energy extraction with hyperbolic metamaterials, *Nano Lett.* 15, 1217 (2015).
- [13] C. Lucchesi, D. Cakiroglu, J.-P. Perez, T. Taliercio, E. Tournié, P.-O. Chapuis, and R. Vaillon, Near-field thermophotovoltaic conversion with high electrical power density and cell efficiency above 14%, *Nano Lett.* 21, 4524 (2021).
- [14] V. Yannopapas and N. V. Vitanov, Spatiotemporal control of temperature in nanostructures heated by coherent laser fields, *Phys. Rev. Lett.* 110 (2013).
- [15] G. P. Zograf, M. I. Petrov, D. A. Zuev, P. A. Dmitriev, V. A. Milichko, S. V. Makarov, and P. A. Belov, Resonant nonplasmonic nanoparticles for efficient temperature-feedback optical heating, *Nano Lett.* 17, 2945 (2017).
- [16] A. Assadillayev, T. Hinamoto, M. Fujii, H. Sugimoto, and S. Raza, Thermal near-field tuning of silicon mie nanoparticles, *Nanophotonics* 10, 4161 (2021).
- [17] X. Zhu, W. Feng, J. Chang, Y.-W. Tan, J. Li, M. Chen, Y. Sun, and F. Li, Temperature-feedback upconversion nanocomposite for accurate photothermal therapy at facile temperature, *Nat. Commun.* 7 (2016).
- [18] P. Ben-Abdallah, S.-A. Biehs, and K. Joulain, Many-body radiative heat transfer theory, *Phys. Rev. Lett.* 107 (2011).
- [19] P. Ben-Abdallah, Multitip near-field scanning thermal microscopy, *Phys. Rev. Lett.* 123 (2019).
- [20] T. X. Hoang, D. Leykam, and Y. Kivshar, Photonic flatband resonances in multiple light scattering, *Phys. Rev. Lett.* 132 (2024).
- [21] B. Müller, R. Incardone, M. Antezza, T. Emig, and M. Krüger, Many-body heat radiation and heat transfer in the presence of a nonabsorbing background medium, *Phys. Rev. B* 95, 085413 (2017).
- [22] T. Agrenius, C. Gonzalez-Ballester, P. Maurer, and O. Romero-Isart, Interaction between an optically levitated nanoparticle and its thermal image: Internal thermometry via displacement sensing, *Phys. Rev. Lett.* 130 (2023).
- [23] A. Narayanaswamy and G. Chen, Thermal near-field radiative transfer between two spheres, *Phys. Rev. B* 77, 075125 (2008).
- [24] A. I. Volokitin and J. Persson, Resonant photon tunneling enhancement of the radiative heat transfer, *Phys. Rev. B* 69 (2004).
- [25] Y. Zhang, J. Wang, F. Wang, Z. Cai, and H.-L. Yi, Enhanced radiative heat transfer via the coupling of multi-particle interactions with combined surface models, *Int. J. Heat Mass Transf.* 215 (2023).
- [26] Y. Zhang, H.-L. Yi, H. Tan, and M. Antezza, Giant resonant radiative heat transfer between nanoparticles, *Phys. Rev. B* 100 (2019).
- [27] J.-L. Fang, X. Luo, L. Qu, and H.-L. Yi, Near-field thermal modulator between nanoparticles based on the multilayered structure, *Int. J. Heat Mass Transf.* 212, 124295 (2023).
- [28] M. Lim, J. Song, S. H. Lee, J. Lee, and B. E. Lee, Surfaceplasmon-enhanced near-field radiative heat transfer between planar surfaces with a thin-film plasmonic coupler, *Phys. Rev. Appl.* 14 (2020).
- [29] R. Messina, M. Antezza, and P. Ben-Abdallah, Three-body amplification of photon heat tunneling, *Phys. Rev. Lett.* 109 (2012).
- [30] P. Ben-Abdallah and S.-A. Biehs, Near-field thermal transistor, *Phys. Rev. Lett.* 112 (2014).

- [31] H. Iizuka and S. Fan, Significant enhancement of near-field electromagnetic heat transfer in a multilayer structure through multiple surface-states coupling, *Phys. Rev. Lett.* 120 (2018).
- [32] J.-P. Mulet, K. Joulain, R. Carminati, and J.-J. Greffet, Nanoscale radiative heat transfer between a small particle and a plane surface, *Appl. Phys. Lett.* 78, 2931 (2001).
- [33] A. Frisk Kockum, A. Miranowicz, S. De Liberato, S. Savasta, and F. Nori, Ultrastrong coupling between light and matter, *Nat. Rev. Phys.* 1, 19 (2019).
- [34] G. Jarc, S. Y. Mathengattil, A. Montanaro, F. Giusti, E. Rigoni, R. Sergo, F. Fassioli, S. Winnerl, S. D. Zilio, D. Mihailović, P. Prelovšek, M. Eckstein, and D. Fausti, Cavity-mediated thermal control of metal-to-insulator transition in 1T-TaS<sub>2</sub>, *Nature* 622, 487 (2023).
- [35] M. Aspelmeier, T. J. Kippenberg, and F. Marquardt, Cavity optomechanics, *Rev. Mod. Phys.* 86, 1391 (2014).
- [36] A. de los Ríos Sommer, N. Meyer, and R. Quidant, Strong optomechanical coupling at room temperature by coherent scattering, *Nat. Commun.* 12 (2021).
- [37] D. Thompson, L. Zhu, E. Meyhofer, and P. Reddy, Nanoscale radiative thermal switching via multi-body effects, *Nat. Nanotechnol.* 15, 99 (2019).
- [38] R. Messina and M. Antezza, Three-body radiative heat transfer and casimir-lifshitz force out of thermal equilibrium for arbitrary bodies, *Phys. Rev. A* 89 (2014).
- [39] S. Khayam and M. Ghashami, Enhancement and suppression of near-field radiative heat transfer in planar many-body systems, *Phys. Rev. B* 110 (2024).
- [40] J.-P. Mulet, K. Joulain, R. Carminati, and J.-J. Greffet, Enhanced radiative heat transfer at nanometric distances, *Microscale Thermophys. Eng.* 6, 209 (2002).
- [41] R. L. Heinisch, F. X. Bronold, and H. Fehske, Mie scattering by a charged dielectric particle, *Phys. Rev. Lett.* 109 (2012).
- [42] S.-A. Biehs, E. Rousseau, and J.-J. Greffet, Mesoscopic description of radiative heat transfer at the nanoscale, *Phys. Rev. Lett.* 105 (2010).
- [43] M. Francoeur, M. P. Mengüç, and R. Vaillon, Local density of electromagnetic states within a nanometric gap formed between two thin films supporting surface phonon polaritons, *J. Appl. Phys.* 107 (2010).
- [44] L. Novotny and B. Hecht, *Principles of Nano-Optics* (Cambridge University Press, 2006).
- [45] K. Asheichyk and M. Krüger, Radiative heat transfer with a cylindrical waveguide decays logarithmically slow, *Phys. Rev. Lett.* 129 (2022).
- [46] K. Asheichyk, B. Müller, and M. Krüger, Heat radiation and transfer for point particles in arbitrary geometries, *Phys. Rev. B* 96 (2017).
- [47] S. Albaladejo, R. Gómez-Medina, L. S. Froufe-Pérez, H. Marinchio, R. Carminati, J. F. Torrado, G. Armelles, A. García-Martín, and J. J. Sáenz, Radiative corrections to the polarizability tensor of an electrically small anisotropic dielectric particle, *Opt. Express* 18, 3556 (2010).
- [48] See supplemental material at [url] for the necessary equations for computing the interface transfer coefficients and reflection coefficients, as well as discussions on the properties of the slab materials, the wavenumber selection mechanism, the influence of repeater thickness and the control of asymmetric reflectors.
- [49] E. D. Palik, *Handbook of optical constants of solids*. 2 (Boston Acad. Press, 2003).
- [50] K. Joulain, J.-P. Mulet, F. Marquier, R. Carminati, and J.-J. Greffet, Surface electromagnetic waves thermally excited: Radiative heat transfer, coherence properties and casimir forces revisited in the near field, *Surf. Sci. Rep.* 57, 59 (2005).
- [51] J. Dong, J. Zhao, and L. Liu, Long-distance near-field energy transport via propagating surface waves, *Phys. Rev. B* 97 (2018).
- [52] J.-L. Fang, L. Qu, Y. Zhang, and H.-L. Yi, Active control of near-field radiative heat transfer between nanoparticles and slab via the multilayered surface modes, *Int. J. Heat Mass Transf.* 200, 123515 (2023).
- [53] M. Francoeur, S. Basu, and S. J. Petersen, Electric and magnetic surface polariton mediated near-field radiative heat transfer between metamaterials made of silicon carbide particles, *Opt. Express* 19, 18774 (2011).
- [54] Q. Zhao, J. Zhou, F. Zhang, and D. Lippens, Mie resonance-based dielectric metamaterials, *Mater. Today* 12, 60–69 (2009).
- [55] G. T. Papadakis, C. J. Ciccarino, L. Fan, M. Orenstein, P. Narang, and S. Fan, Deep-subwavelength thermal switch via resonant coupling in monolayer hexagonal boron nitride, *Phys. Rev. Appl.* 15 (2021).
- [56] L. Xie and B. Song, Isotope effect on radiative thermal transport, *Phys. Rev. B* 107 (2023).
- [57] K. Asheichyk and M. Krüger, Heat radiation and transfer in confinement, *Phys. Rev. B* 98 (2018).
- [58] K. Asheichyk, P. Ben-Abdallah, M. Krüger, and R. Messina, Long-range super-planckian heat transfer between nanoemitters in a resonant cavity, *Phys. Rev. B* 108, 155401 (2023).
- [59] Y. Zhang, J. Dong, G. Tang, and H.-L. Yi, Many-particle radiative heat transfer in a nonreciprocal graphene plasmonic cavity, *Phys. Rev. B* 103 (2021).
- [60] S. Shen, A. Narayanaswamy, and G. Chen, Surface phonon polaritons mediated energy transfer between nanoscale gaps, *Nano Lett.* 9, 2909 (2009).
- [61] P. Ben-Abdallah, R. Messina, S.-A. Biehs, M. Tschikin, K. Joulain, and C. Henkel, Heat superdiffusion in plasmonic nanostructure networks, *Phys. Rev. Lett.* 111 (2013).
- [62] I. Latella, R. Messina, S. Biehs, J. M. Rubí, and P. Ben-Abdallah, Saturation of radiative heat transfer due to many-body thermalization, *Sci. Rep.* 10 (2020).
- [63] S.-A. Biehs and P. Ben-Abdallah, Near-field heat transfer between multilayer hyperbolic metamaterials, *Z. Naturforsch. A* 72, 115 (2016).
- [64] I. Latella, P. Ben-Abdallah, S.-A. Biehs, M. Antezza, and R. Messina, Radiative heat transfer and nonequilibrium casimir-lifshitz force in many-body systems with planar geometry, *Phys. Rev. B* 95 (2017).
- [65] R. Chikkaraddy, B. de Nijs, F. Benz, S. J. Barrow, O. A. Scherman, E. Rosta, A. Demetriadou, P. Fox, O. Hess, and J. J. Baumberg, Single-molecule strong coupling at room temperature in plasmonic nanocavities, *Nature* 535, 127 (2016).
- [66] K. Santhosh, O. Bitton, L. Chuntunov, and G. Haran, Vacuum rabi splitting in a plasmonic cavity at the single quantum emitter limit, *Nat. Commun.* 7 (2016).
- [67] O. Ilic, N. H. Thomas, T. Christensen, M. C. Sherrott, M. Soljačić, A. J. Minnich, O. D. Miller, and H. A. Atwater, Active radiative thermal switching with graphene plasmon resonators, *ACS Nano* 12, 2474 (2018).

- [68] S. Lang, M. Tschikin, S. Biehs, A. Y. Petrov, and M. Eich, Large penetration depth of near-field heat flux in hyperbolic media, *Appl. Phys. Lett.* 104 (2014).
- [69] S.-A. Biehs, M. Tschikin, and P. Ben-Abdallah, Hyperbolic metamaterials as an analog of a blackbody in the near field, *Phys. Rev. Lett.* 109 (2012).
- [70] P. Chapuis, B. J. Lee, and A. W. Rodríguez, Thermal radiation at the nanoscale and applications, *Appl. Phys. Lett.* 123 (2023).
- [71] M. Pascale, M. Giteau, and G. T. Papadakis, Perspective on near-field radiative heat transfer, *Appl. Phys. Lett.* 122 (2023).
- [72] J. Rieser, M. A. Ciampini, H. Rudolph, N. Kiesel, K. Hornberger, B. A. Stickler, M. Aspelmeyer, and U. Delić, Tunable light-induced dipole-dipole interaction between optically levitated nanoparticles, *Science* 377, 987 (2022).
- [73] J. Vijayan, J. Piotrowski, C. Gonzalez-Ballester, K. Weber, O. Romero-Isart, and L. Novotny, Cavity-mediated long-range interactions in levitated optomechanics, *Nat.Phys.* (2024).
- [74] H. Salihoglu, J. Shi, Z. Li, Z. Wang, X. Luo, I. V. Bondarev, S. Biehs, and S. C. Shen, Nonlocal near-field radiative heat transfer by transdimensional plasmonics, *Phys. Rev. Lett.* 131 (2023).
- [75] S. Biehs and I. V. Bondarev, Far- and near-field heat transfer in transdimensional plasmonic film systems, *Adv. Opt. Mater.* 11 (2023).
- [76] P. Ben-Abdallah and A. W. Rodríguez, Controlling local thermal states in classical many-body systems, *Phys. Rev. Lett.* 129 (2022).
- [77] S.-A. Biehs and P. Ben-Abdallah, Heat transfer mediated by the berry phase in nonreciprocal many-body systems, *Phys. Rev. B* 106 (2022).
- [78] Z. Xu, P. Ju, X. Gao, K. Shen, Z. Jacob, and T. Li, Observation and control of casimir effects in a sphere-plate system, *Nat. Commun.* 13 (2022).
- [79] M. Krüger, T. Emig, G. Bimonte, and M. Kardar, Non-equilibrium casimir forces: Spheres and sphere-plate, *Europhys. Lett.* 95, 21002 (2011).